Received: 23 June 2016 | Revised: 15 November 2016 | Accepted: 22 December 2016

DOI: 10.1002/stc.1991

WILEY

RESEARCH ARTICLE

Improved semi-active control algorithm for hydraulic damper-based braced buildings

Mohsen Azimi[1] | Akbar Rasoulnia[2] | Zhibin Lin[1] | Hong Pan[1]

[1] Department of Civil and Environmental Engineering, North Dakota State University, Fargo, North Dakota 58105, USA

[2] Department of Civil Engineering, Sharif University of Technology, Tehran, Iran

Correspondence
Zhibin Lin, Department of Civil and Environmental Engineering, North Dakota State University, Fargo, North Dakota 58105, USA.
Email: zhibin.lin@ndsu.edu

Summary

Much research has been conducted on structural control systems to improve the seismic performance of structures under earthquakes and, ultimately, offer high performance-resilient buildings beyond life risk mitigation. Among various structural control algorithms, semi-active control strategies have been widely accepted for overcoming some limitations existed in either passive or active control systems, thereby leading to better structural performance over their counterparts. In this study, a new semi-active control algorithm with minimum control parameters is developed to drive the hydraulic damper for effective control of the dynamic deformation of low- and high-rise building structures under earthquake loadings. The new controller allows less input and computation for determining the damping coefficient of the hydraulic dampers while maintaining a higher performance. V-braced buildings with three varying heights are used as prototypes to demonstrate the effectiveness of the proposed semi-active damper. Two critical parameters, maximum drift and acceleration of stories, are defined for the performance criteria. The simulation results show that the developed semi-active damper can significantly improve the seismic performance of the buildings in terms of controlled story drift and acceleration. By use of less input and reduced time delay effects, the proposed control system is comparable with those of existing semi-active controllers. The findings in this study will help engineers to design control systems for seismic risk mitigation and effectively facilitate the performance-based seismic design.

KEYWORDS

hydraulic damper, LQR, optimal control, semi-active control, V-braced building

1 | INTRODUCTION

Buildings are vulnerable to severe vibration when subjected to extreme hazard events, such as earthquakes and winds. A typical building design is to prevent collapse in terms of expected deformation or stress demands to structural components in the event of earthquakes.[1] Practicing engineers have long recognized that structural response of buildings to strong ground motion due to earthquakes or other extreme events frequently results in inelastic behavior.[2] There is, however, very limited and small inherent damping of conventional building materials and structural components to allow dissipating such considerable dynamic energy.[3] As a result, the buildings usually have to behave with substantial damage and possibly permanent deformation. Currently, major earthquakes, such as Sichuan earthquake in China (2008), Christchurch earthquake in New Zealand (2011), Chile earthquake (2010), and Great Sendai earthquake in Japan (2011) confirm this big concern of modern seismic design concept for resilience of buildings and bridges.[4–7]

Research on innovative designs and materials for new and existing buildings has demonstrated their enhanced seismic performance.[8,9] These design approaches mainly include (a) using base isolation concepts or devices to control and reduce the demand,[10,11] (b) using shape memory alloy,[12,13] expansion concrete[14] or post-tensioning active confinement[15] to minimize or eliminate permanent deformation, and (c) using jacketing[16,17] through passive confinement to

increase ductility capacity. Considering that in performance-based engineering, it is required that a building structure achieves multiple performance levels under small, moderate, and strong earthquakes;[18] these methods and techniques, however, cannot provide sufficient adaptability and may even lead to uneconomic design in order to accommodate different performance levels.[19,20]

Alternatively, increasing efforts in recent years have been directed to the development and implementation of control systems for higher seismic performance and enhanced resilience of buildings.[21–23] A control system usually refers to control algorithms (e.g., active control, semi-active control, hybrid control, and passive control[24–26]) and the corresponding controlling devices (e.g., semi-control hydraulic dampers and active-control piezoelectric actuators[27]). Among various control algorithms, semi-active control systems exhibit their attractive characteristics, including less power, higher reliability, and particularly higher adaptability for earthquake events, as compared to their counterparts.[25,26,28–31] As a result, semi-active control systems and the associated devices have played an important role in structural vibration controls and mitigations.

The full-scale semi-active control system was first implemented to the Kajima Shizuoka Building in 1998, in Shizuoka, Japan.[32] Two semi-active hydraulic dampers were installed at the first to fourth stories, while linear quadratic regulator (LQR) was used as a controlling algorithm to adjust damping forces. After that, there are many cases worldwide with a high variety in use of semi-active control systems and hydraulic dampers.[31,33,34] Kurino et al.[35] studied semi-active and passive control systems with dampers under different levels of earthquakes. The dampers in their systems were controlled by the Maxwell's model to allow generating two maximum and minimum damping forces for accommodating different levels of seismic response. In this method, the damper can be adjusted to either its high- or low-state damping that may use simpler algorithms but does not generate continuous damping. Note that semi-active hydraulic damper systems in those studies were mainly driven by on–off bi-mode to switch valves for controlling damping forces to structures.[36]

Other researchers[37] applied optimization techniques into their studies to achieve reduction in maximum response with minimum cost. Cundumi and Suárez[37] proposed a variable semi-active damping device, consisting of two fixed-orifice viscous fluid dampers. The developed damper was mounted to the frame by one end while the other side was a moving end along a connected collar. The position of the moving end was driven using an actuator with a modified LQR algorithm, by which a performance index in the state vector was minimized to control the structural vibration. Similarly, Kazemi Bidokhti et al.[38] investigated seismic performance of three- and 10-story buildings strengthened by semi-active hydraulic dampers on their V-bracing members. The genetic algorithm was selected in their study for optimizing the dampers, in which the input parameters were displacement, velocity, and acceleration of each story, and the output was the damping required for the devices. Their results revealed that the proposed control system was efficient in seismic risk mitigation by considerable reduction in structural displacements, velocities, and accelerations. One challenge of such controlling algorithm in its actual implementation, however, was computational capability and time consumption for data processing and optimization of the input variables and yielding damping coefficients instantaneously. Shih et al.[39] have recently proposed a semi-active hydraulic damper as an active interaction control device. The dampers in their study were placed between story levels, and the substructure was simulated as a single degree of freedom system with damping and stiffness. As a result, the damping force was obtained based on the inter-story velocity. Clearly, the steps were still quite time consuming.

These dampers and algorithms are still under development and are gaining more attention because of their superior compatible characteristics.[40,41] Clearly, most of the recently developed algorithms for controlling the hydraulic dampers are based on on–off control techniques.[42–44] These algorithms are simple but require many input data and computation time if there is any attempt for generating continuous damping coefficients.

This study, therefore, is to introduce a control system with semi-active damper that determines the controlling damping force without using complicated algorithms. The proposed controller for obtaining the damping coefficients of the hydraulic dampers requires much less computation, while maintaining good performance. The damping coefficients are derived from force–displacement equilibrium equations of the bracing and the damper that can eliminate the undesired bracing flexibility effects on the responses. The only input data for the proposed control system is the strain of the bracing members during an excitation. The effectiveness of the proposed system is then demonstrated by an implementation to three (1-, 5-, and 10-story) buildings, and the time delay effects on the control system are also studied.

2 | DESIGN OF INTEGRATED BRACING FLEXIBILITY COMPENSATOR (IBFC) CONTROL SYSTEM

Figure 1 displays the schematics of the proposed control system; the control algorithm is given in Figure 2. The main concept is to reduce input parameters for determining damping coefficients, while maintaining overall acceptable performance. The parameters, m_i and m_{i+1} in Figure 1, represent the story masses. Subscriptions d, b, and s correspond to damper, bracing, and stiffness of the frame, respectively. As schematically illustrated in Figure 1, the strain of the bracing in this system is collected from mounted sensors and sent to the controller as input data. Then, the damping coefficient

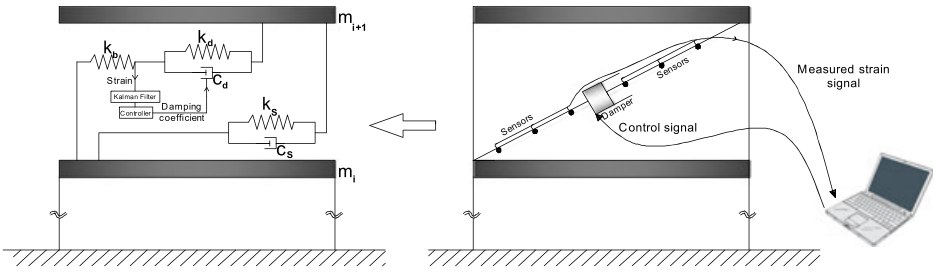

FIGURE 1 Mechanical model of the control system

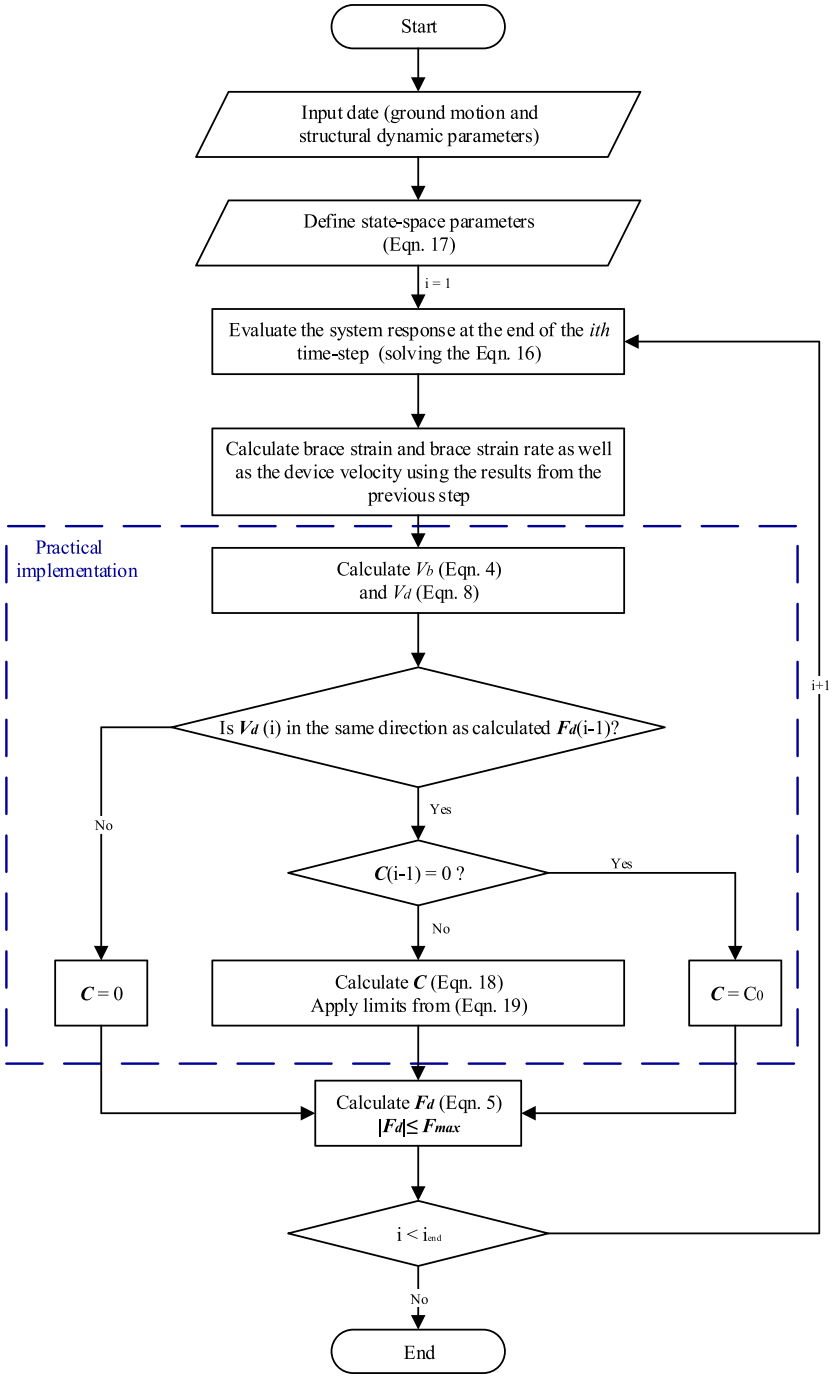

FIGURE 2 Flowchart of the proposed control strategy

is determined by a microprocessor using the proposed controller (see Figure 1).

The inter-story velocity is defined as the summation of the damper shaft velocity and the bracing velocity,

$$V_d(t) + V_b(t) = V_{in}(t), \tag{1}$$

where $V_b(t)$, $V_d(t)$, and $V_{in}(t)$ are the bracing velocity, the damper shaft velocity, and the inter-story velocity, respectively. The device damping coefficient, $C(t)$, is defined based on a previous study by Ahmadizadeh[45] for the effects of flexibility of bracing members on the control systems with hydraulic dampers, in which dampers were directly connected to bracing members in series:

$$C(t) = C_0 \frac{V_{in}(t)}{V_d(t)}, \tag{2}$$

where C_0 is constant. This concept tends to eliminate the undesired effects of the bracing flexibility on the overall performance of the system when it is connected in series with the damper.[45]

Thus, introducing Equation 1 in Equation 2 yields

$$C(t) = C_0 \frac{V_d(t) + V_b(t)}{V_d(t)} = C_0 \left(1 + \frac{V_b(t)}{V_d(t)}\right). \tag{3}$$

The velocity of the bracing is then calculated with respect to its strain rate as follows:

$$V_b(t) = \frac{\Delta l_b(t)}{\Delta t} = \frac{\Delta \varepsilon_b(t) \times l_b}{\Delta t} = \dot{\varepsilon}_b(t) \times l_b, \tag{4}$$

where l_b is the bracing length, $\Delta l_b(t)$ is the bracing elongation in a time step of Δt, $\varepsilon_b(t)$ is the strain of the bracing, and $\dot{\varepsilon}_b(t)$ is the strain rate of the bracing. The damping of the controller and axial forces of the bracing members will be generated from their definitions:

$$F_d(t) = V_d(t) \times C(t), \tag{5}$$

$$F_b(t) = k_{eq} \times \Delta l_b(t) = k_{eq} \times \varepsilon(t) \times l, \tag{6}$$

in which $F_d(t)$ is the damping force, $F_b(t)$ is the bracing force, and k_{eq} is the equivalent stiffness for the bracing and the damper when they are in series:

$$k_{eq} = \frac{k_b \times k_d}{k_b + k_d}, \tag{7}$$

where k_b and k_d are the bracing stiffness and damper shaft stiffness, respectively. Consider that the bracing and the damper are connected in series, both have identical axial forces and thus, the velocity of the damper shaft can be derived by equating the right-hand sides of Equations 5 and 6:

$$V_d(t) = \frac{k_{eq} \times \varepsilon_b(t) \times l_b}{C(t)}. \tag{8}$$

Note that the length of the damper shaft is neglected mainly provided that it is relatively small as compared to the entire length of the bracings. Substituting the velocities of both damper and the bracing in Equations 4 and 8 in Equation 3 will give the damping coefficient in the form:

$$C(t) = C_0 \left[1 + \frac{\dot{\varepsilon}_b(t)}{k_{eq} \times \varepsilon_b(t)} C(t)\right], \tag{9}$$

or reorganizing Equation 9 as

$$C(t) = \frac{C_0}{1 - \frac{\dot{\varepsilon}_b(t) \times C_0}{k_{eq} \times \varepsilon_b(t)}}. \tag{10}$$

As clearly shown in Equation 10, all the parameters are constant, except the strain $\varepsilon_b(t)$ and the strain rate $\dot{\varepsilon}_b(t)$ of the bracing member. The strain rate is an implicit function of the strain that is derived from a set of data points to compute their first derivative: at the ith step, by substituting the Equations 4 and 8 into Equation 1, the strain rate $\dot{\varepsilon}_b^i(t)$ of the bracing members can be derived by

$$\dot{\varepsilon}_b^i(t) = V_{in}^i / L_b - k_{eq} \varepsilon_b^i / C^{i-1}. \tag{11}$$

Therefore, the only input parameter is the strain of the bracing member. Note that the collected sensor data could be contaminated by various operational conditions, such as noise interference. The effects of the noise to data and data fusion for noise removal are addressed later in Section 6. Detailed implementation of the proposed methods in conventional frame buildings and their dynamic governing equations are demonstrated in the following sections.

3 | IMPLEMENTATION OF THE PROPOSED CONTROL SYSTEM IN BUILDINGS

3.1 | Governing equations of building with semi-active control system

The dynamic governing equations of a building are usually described in matrix form[46] when subjected to a ground motion, $\ddot{x}_g$:

$$[\boldsymbol{M}]\{\ddot{x}(t)\} + [\boldsymbol{C}]\{\dot{x}(t)\} + [\boldsymbol{K}]\{x(t)\} = -[\boldsymbol{M}]\{\boldsymbol{E}\}\ddot{x}_g(t), \tag{12}$$

where $\boldsymbol{M}$, $\boldsymbol{C}$, and $\boldsymbol{K}$ are the mass, damping, and stiffness matrices and $\{x\}$, $\{\dot{x}\}$, $\{\ddot{x}\}$ are the nodal displacement, velocity, and acceleration vectors, respectively. $\boldsymbol{E}$ is the influence

factor that is a vector of all ones in this case, and n is the number of degrees of freedom. The Rayleigh method is used to get the damping matrix based on the mass and stiffness matrices.[47] An inherent damping of 2% is assumed for the first two modes of vibration.

Similarly, the dynamic governing equations of the building installed with a control system[46] are thus defined by a conventional dynamic system with a contribution of a controller:

$$[\boldsymbol{M}]\{\ddot{x}(t)\} + [\boldsymbol{C}]\{\dot{x}(t)\} + [\boldsymbol{K}]\{x(t)\} = [\boldsymbol{D}]\{u(t)\} - [\boldsymbol{M}]\{\boldsymbol{E}\}\ddot{x}_g(t), \tag{13}$$

where $\{u(t)\}$ is the controlling force vector; $\boldsymbol{D}$ is the $(n \times r)$ matrix defined for the location of the controllers in the building[8,9]; n and r are the number stories and number of dampers used, respectively.

$$\boldsymbol{D} = \begin{bmatrix} & & & & \\ 1 & -1 & & & \\ & 1 & -1 & & \\ & & 1 & -1 & \\ & & & \ddots & \ddots \\ & & & & \ddots \end{bmatrix}. \tag{14}$$

To solve the differential equation of motion in Equation 13, it is convenient to rewrite the governing equations in Equation 13 in state–space form:

$$\begin{aligned}\{\ddot{x}(t)\} = &-[\boldsymbol{M}]^{-1}[\boldsymbol{K}]\{x(t)\} - [\boldsymbol{M}]^{-1}[\boldsymbol{C}]\{\dot{x}(t)\} \\ &+ [\boldsymbol{M}]^{-1}[\boldsymbol{D}]\{u(t)\} - \{\boldsymbol{E}\}\ddot{x}_g(t),\end{aligned} \tag{15a}$$

and the velocity vector, $\dot{x}$, is rewritten by

$$\{\dot{x}(t)\} = [\boldsymbol{I}]\{\dot{x}(t)\}. \tag{15b}$$

Thus, Equations 15a and 15b are expanded in a $2n \times 1$ vector by

$$\begin{aligned}\begin{Bmatrix}\{\dot{x}(t)\} \\ \{\ddot{x}(t)\}\end{Bmatrix} = &\begin{bmatrix}[0] & [\boldsymbol{I}] \\ -[\boldsymbol{M}]^{-1}[\boldsymbol{K}] & -[\boldsymbol{M}]^{-1}[\boldsymbol{C}]\end{bmatrix}\begin{Bmatrix}\{x(t)\} \\ \{\dot{x}(t)\}\end{Bmatrix} \\ &+ \begin{bmatrix}[0] \\ [\boldsymbol{M}]^{-1}[\boldsymbol{D}]\end{bmatrix}\{u(t)\} + \begin{Bmatrix}\{0\} \\ -\{\boldsymbol{E}\}\end{Bmatrix}\ddot{x}_g(t).\end{aligned} \tag{16}$$

The second-order equation of motion for the system in Equation 13 is reduced in a first-order state-variable as

$$\{\dot{z}(t)\} = [\boldsymbol{A}]\{z(t)\} + [\boldsymbol{B}]\{u(t)\} + \{\boldsymbol{H}\}\ddot{x}_g, \tag{17a}$$

where $\{z(t)\}$ is the $(2n \times 1)$ state-vector and the matrices, $\boldsymbol{A}$, $\boldsymbol{B}$, and $\boldsymbol{H}$, are defined below.

$$\{z(t)\} = \begin{Bmatrix} x(t) \\ \dot{x}(t) \end{Bmatrix}; \tag{17b}$$

$$\begin{aligned}\boldsymbol{A} = \begin{bmatrix} 0 & \boldsymbol{I} \\ -\boldsymbol{M}^{-1}\boldsymbol{K} & -\boldsymbol{M}^{-1}\boldsymbol{C} \end{bmatrix};\ \boldsymbol{B} = \begin{bmatrix} 0 \\ \boldsymbol{M}^{-1}\boldsymbol{D} \end{bmatrix};\boldsymbol{H} \\ = \begin{bmatrix} 0 \\ -\{\boldsymbol{E}\} \end{bmatrix}.\end{aligned} \tag{17c}$$

Thus, the solutions of this first-order differential state–space equation are determined based on numerical methods developed in the literature.[9]

3.2 | Implementation of the proposed control algorithm

3.2.1 | Proposed IBFC control algorithm

To determine the controlling force, the proposed control algorithm IBFC developed in Section 2 needs to be predefined, and a flowchart is herein generated to frame on how to implement the control algorithm in the whole system, as shown in Figure 2. The control algorithm is programmed based on this flowchart. The input data (i.e., mass, stiffness, damping matrices, as well as earthquake record, and state–space parameters) are defined. Then, the response of the structure enables one to compute bracing strain and brace strain rate at each time step, which allows determining the new damping coefficients $\boldsymbol{C}$ of the whole system and control forces that can be easily adjustable by changing device input voltage.

The determination of the control forces, illustrated in Figure 2, needs to be solved by iterations, in which the steps are described as follows:

Step 1. Assemble the dynamic system in Equation 13 and state–space parameters in Equation 17a with input data;

Step 2. Calculate structural response, $x^i(t)$ and $\dot{x}^i(t)$, at the ith step from solving the first-order differential state–space equations in Equation 17a. As such, the strain $\varepsilon_b^i(t)$ is determined according to the collected data from mounted sensors, while the strain rate $\dot{\varepsilon}_b^i(t)$ of the bracing member is determined by $\dot{\varepsilon}_b^i(t) = V_{in}^i/L_b - k_{eq}\varepsilon_b^i/C^{i-1}$ in Equation 11.

Step 3. Calculate the velocity of the bracing $V_b^i(t)\left(=\dot{\varepsilon}_b^i(t)\times l_b\right)$ in Equation 4 and the velocity of the device $V_d^i(t) = k_{eq}\times\varepsilon_b^i(t)\times l_b/C^{i-1}(t)$ in Equation 8 and check if the direction of the $V_d^i(t)$ is the same as that of the control force $F_d^{i-1}(t)$ at the previous step; moving to Step 4 if yes. Otherwise, $C^i(t) = 0$ and skip to Step 6.

Step 4. Calculate the damping coefficient, $C^i(t)$, of the each damper in Equation 9 according to the damping coefficient at the previous step;

$$C^i(t) = C_0\left[1 + \frac{\dot{\varepsilon}_b^i(t)}{k_{eq}\times\varepsilon_b^i(t)}C^{i-1}(t)\right]. \quad (18)$$

Step 5. Check limitation for $C^i(t)$ according to the equation below, while damping coefficient of each damper is determined based on the desired control force and the capacity of each device:

$$C^i(t) = \begin{cases} F_{\max}/|v_i(t)| & u_i(t)\times v_i(t) > 0, |u_i(t)| > F_{\max} \\ C_{\max}, & u_i(t)\times v_i(t) > 0, \left|{}^{u_i(t)}/_{v_i(t)}\right| > C_{\max}, |u_i(t)| \le F_{\max} \\ u_i(t)/v_i(t) & u_i(t)\times v_i(t) > 0, \left|{}^{u_i(t)}/_{v_i(t)}\right| \le C_{\max}, |u_i(t)| \le F_{\max} \\ 0 & u_i(t)\times v_i(t) \le 0 \end{cases}, \quad (19)$$

where $u_i(t)$ and $v_i(t)$ are the desired control force and the velocity of each damper at ith time step, respectively. $F_{\max}$ and $C_{\max}$ are the maximum damping force and the damping coefficient of each damper ($F_{\max} = 900$ kN and $C_{\max} = 200\times10^6$ N.s.m^{-1}), respectively. For the passive system, the damping coefficient is obtained based on the performance index of the system, as later discussed in Section 5.

Step 6. Calculate the damping control forces $F_d^i(t)$ $\left(= V_d^i(t)\times C^i(t)\right)$ in Equation 5;

Step 7. Repeat Steps 2 through 6 until the last time step of the ground motion.

LQR control algorithm: In order to evaluate effectiveness of the proposed IBFC, semi-active system with the LQR algorithm, which has been developed by Kurata et al.,[32] was used to compare the results. LQR is widely used in optimum control techniques in structural control problems[48–55] that finds an active control parameters to minimize the cost function given by the form:

$$J = \frac{1}{2}\int_0^\infty \left(\{z(t)\}^T[\boldsymbol{Q}]\{z(t)\} + \{u(t)\}^T[\boldsymbol{R}]\{u(t)\}\right) dt. \quad (20)$$

The weighting matrices for the semi-active LQR method, $\boldsymbol{Q}$, and $\boldsymbol{R}$ are chosen as

$$\boldsymbol{Q} = \begin{bmatrix} \boldsymbol{I}_{n\times n} & \boldsymbol{O} \\ \boldsymbol{O} & \boldsymbol{I}_{n\times n} \end{bmatrix}\times Q_n, \boldsymbol{R} = [\boldsymbol{I}_{r\times r}]\times R_n, \quad (21)$$

where n and r are the number of stories and controllers. Q_n and R_n are the coefficients that are selected using optimization procedure in order to get the maximum reduction in the responses. For example, these two parameters, Q_n and R_n, are given in a vector form, in which the rows represent the one-story, five-story, and 10-story buildings used in numerical examples.

$$Q_n = \begin{bmatrix} Q_{n=1} \\ Q_{n=5} \\ Q_{n=10} \end{bmatrix} = \begin{bmatrix} 4.0 \\ 2.4 \\ 4.0 \end{bmatrix}\times10^7, R_n = \begin{bmatrix} R_{n=1} \\ R_{n=5} \\ R_{n=10} \end{bmatrix} = \begin{bmatrix} 0.0002 \\ 0.03 \\ 3.5 \end{bmatrix}\times10^{-6} \quad (22)$$

Thus, the optimal control force vector at each step is

$$\{u_{opt}(t)\} = -[\boldsymbol{G}]\times\{z(t)\} \quad (23)$$

where the control gain matrix is defined by

$$[\boldsymbol{G}] = [\boldsymbol{R}]^{-1}[\boldsymbol{B}]^T[\boldsymbol{P}], \quad (24)$$

in which $\boldsymbol{P}$ is the Riccati matrix and $\{z(t)\}$ is the state feedback vector.

3.3 | Calibration of the proposed methods

One five-story building used in the literature[32] was selected to calibrate the effectiveness of the proposed concepts. The north–south frame of this building was shown in Figure 3b. The building was the first structure equipped with semi-active variable damping system with a height of 19.75 m. Two hydraulic dampers (eight dampers in total) were installed to the bracing members of each story from first to fourth floor,[32] while the dampers were controlled by LQR algorithms. The building was modeled for simplicity using lumped masses for the floors while equivalent springs for

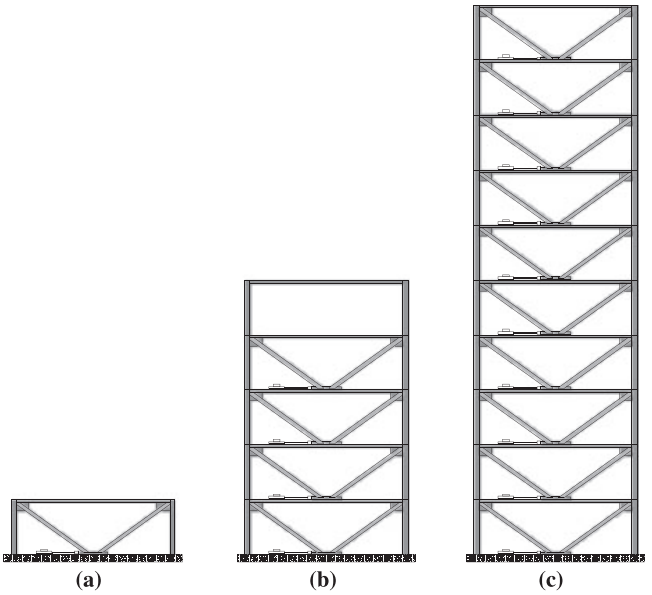

FIGURE 3 Three braced frame buildings with semi-active hydraulic dampers

columns. Structural parameters of this building are listed in Table 1.

Maximum responses at each floor, including the maximum story drift and the peak absolute acceleration, were computed using the proposed methods in Equations 1–18, while the output data were compared with the results predicted by Ahmadizadeh.[45] Figure 4 shows the simulation results for the maximum story drift (see Figure 4a) and the peak absolute acceleration (see Figure 4b) for the five-story building under the El Centro earthquake. The proposed method accurately captured both maximum story drift and the peak absolute acceleration for each floor of the five-story building (with the prediction shown in solid lines and the results from the work of Ahmadizadeh[45] shown in dashed lines), as compared to the previous study.[45]

4 | NUMERICAL SIMULATION USING THE PROPOSED METHODS

Further verification and exploration of the proposed control algorithm were conducted through numerical simulation in this section. Three different multistory buildings were used to demonstrate the effectiveness of the proposed control algorithm in terms of peak response, performance index, and time delay effects, as discussed in detail in Section 5.

TABLE 1 Structural properties of three buildings

Story		Mass (kg)	Stiffness without bracing (kN/mm)	Stiffness of bracing (kN/mm)	Stiffness of damper (kN/mm)	Equivalent stiffness (kN/mm)
One-story	1st	215,200	31.24	1,130	800	468.39
Five-story	5th	266,100	84			
	4th	204,800	89	1,130	800	468.39
	3rd	207,000	99	1,130	800	468.39
	2nd	209,200	113	1,130	800	468.39
	1st	215,200	147	876	800	418.14
Ten-story	10th	230,400	31.24	1,130	800	468.39
	9th	230,400	59.84	1,130	800	468.39
	8th	230,400	63.84	1,130	800	468.39
	7th	230,400	76.69	1,130	800	468.39
	6th	230,400	80.76	1,130	800	468.39
	5th	230,400	93.84	1,130	800	468.39
	4th	230,400	96.61	1,130	800	468.39
	3rd	230,400	97.80	1,130	800	468.39
	2nd	230,400	121.68	1,130	800	468.39
	1st	30,960	162.36	1,130	800	468.39

4.1 | Numerical examples

Three buildings with different stories varying from one to 10 stories (see Figure 3) were selected to calibrate the effectiveness of the proposed control system with semi-active LQR controller for low-, mid-, and high-rise buildings.

One-story building: this building was installed with a semi-active control system with a hydraulic damper as shown in Figure 3a. This building was simulated as a single degree of freedom system with lumped mass at the floor level. Columns were modeled using equivalent springs. Mass, stiffness, and other properties of the frame, as well as damper parameters are given in Table 1.

Five-story building: An analytical model of the actual five-story building that has been studied by Kurata et al.[32] was used in this paper. This building is the first structure equipped with semi-active variable damping system. The height of the building is 19.75 m. This building was designed according to the Japanese building codes. In this building, for each of the first four floors, two dampers (eight dampers in total) were installed to the bracing members. These dampers were controlled by means of LQR algorithms. To control the structural vibration, sensors measure the response of the structure; then, a computer determines the damping force and sends the results to the dampers to generate the required force. The analytical model of the north–south frame of this building was created with semi-active hydraulic dampers as shown in Figure 3b. In order to reduce the analysis time, floors were simplified with lumped masses, and other frame members were simulated using equivalent springs. Structural parameters of this building are given in Table 1.

Ten-story building: In this building, similar to the previous models, the structure (Figure 3c) was considered as a shear frame, in which the floors were assumed more rigid as compared to the stiffness of the columns. Mass and stiffness properties of this model are given in Table 1.

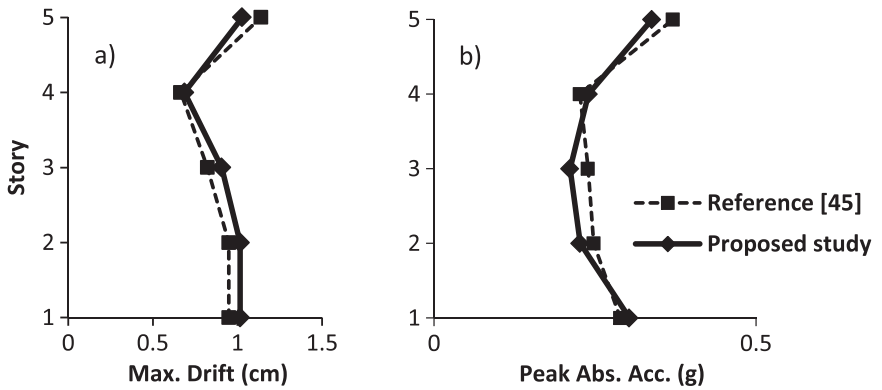

FIGURE 4 Comparison of responses predicted by the proposed method with results in the work of Ahmadizadeh

4.2 | Dynamic analysis and response of the buildings with control systems

The selected three buildings in Section 4.1 were installed with semi-active hydraulic dampers, while the assembly of the dynamic governing equations was presented in Equation 13. Besides the proposed IBFC controller, passive system with optimum damping, and semi-active control systems with the LQR[45] as well as uncontrolled ones were chosen as control systems placed on these buildings for a comparison. Two representative earthquake ground motions were selected as the input variables to the buildings, as listed in Table 2. Note that selection of the ground motions is not the major objectives in this study, and only two ground motions were chosen for simplicity to demonstrate the proposed concept, although more various ground motions could be used to gain more information of structural response and characterize the corresponding control strategies.

Dynamic analysis of the buildings with the proposed control algorithms was conducted in accordance with the flowchart shown in Figure 2. Data outputs, particularly maximum drift and maximum acceleration of stories of the buildings during the earthquakes, were utilized as evaluation criteria in this study, and reduction in these responses enables us to determine the performance of different control systems.[38] Performance index and time delay effects were also introduced as criteria, as presented in the following discussions.

5 | RESULTS AND DISCUSSION

5.1 | Peak response

Maximum drift and maximum acceleration of stories of these three buildings during the earthquakes were plotted to demonstrate the effectiveness of the control systems, as illustrated in Figures 5–7, respectively. Figure 5 indicates that the max drift of the one-story building with passive devices exceeds that of the structure with other devices. In addition, the maximum drift of the controlled structure using proposed method has the least value among the other methods (4 and 11% more reduction compared with SA-LQR and passive, respectively). From the peak absolute acceleration graph, the semi-active LQR system has the most reduction in the response (56%). By comparing the control systems, passive control system can improve the response of the one-story building with respect to the uncontrolled structure, but it is not as effective as the proposed method in reducing the drift. The semi-active

TABLE 2 Characteristics of ground motion accelerations used in the analyses

Earthquake	Date	Station	PGA (g)
El Centro	1940/05/19	117 El Centro Array no. 9	0.32
Northridge	1994/01/17	24087 Arleta–Nordhoff Fire Station	0.34

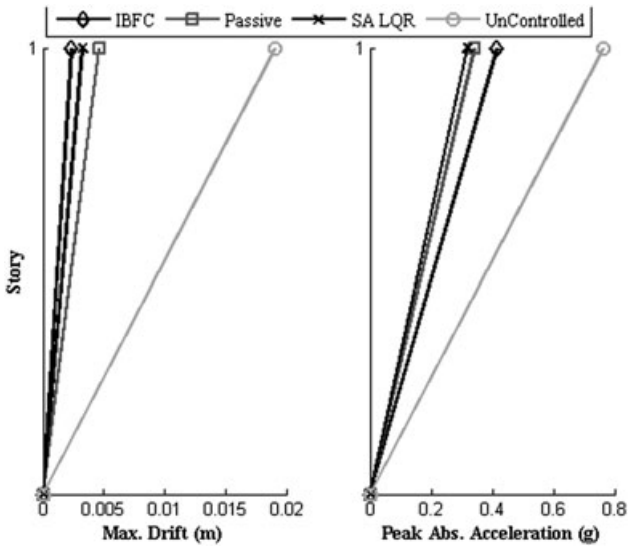

FIGURE 5 Peak response of the one-story building under El Centro earthquake. IBFC = integrated bracing flexibility compensator, SA LQR = semi-active linear quadratic regulator

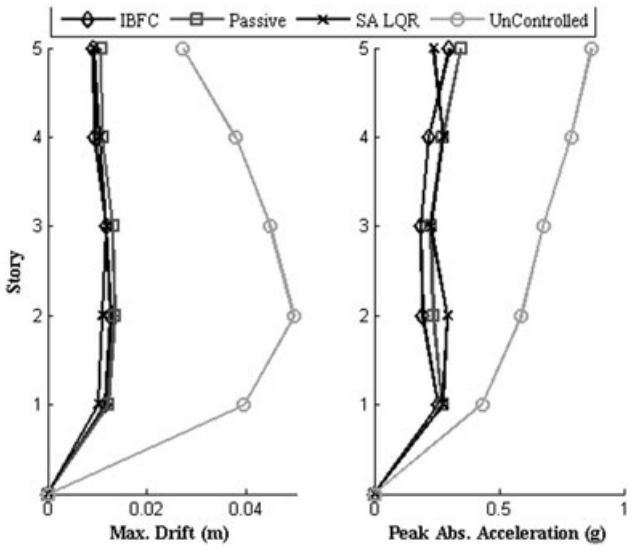

FIGURE 6 Peak response of the five-story building under El Centro earthquake. IBFC = integrated bracing flexibility compensator, SA LQR = semi-active linear quadratic regulator

LQR and IBFC systems have similar responses, but with regard to the complexity of controlling equations and hardware to use, the IBFC can be economical and effective.

For the five-story building, a significant reduction in responses can be obtained using the proposed control system. By comparing the performance of the semi-active LQR and the IBFC systems with passive control, it can be concluded that the proposed control systems provide significant reduction in drift response that is very close to and even smaller than LQR responses. In addition, the IBFC system is very effective in reduction of the peak absolute acceleration. Figures 6 and 7 indicate that for the proposed system, the drift response reduction for the lower stories is close to passive system with optimum damping; however, this system

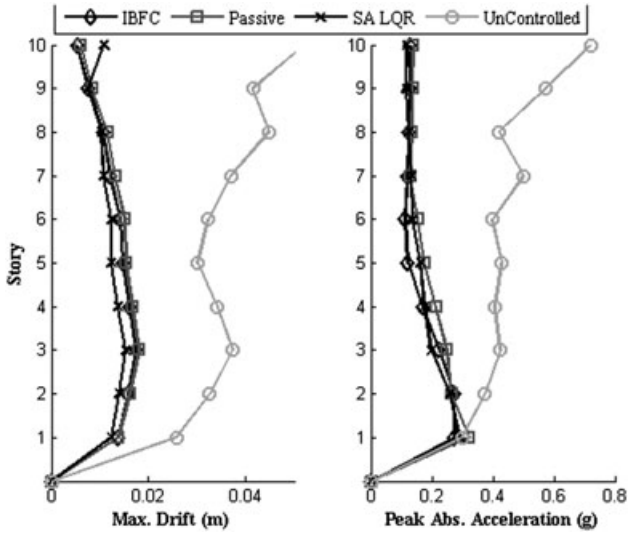

FIGURE 7 Peak response of the 10-story building under El Centro earthquake. IBFC = integrated bracing flexibility compensator, SA LQR = semi-active linear quadratic regulator

provides a better performance in the top floors of the 10-story building. Similarly, the peak absolute acceleration reduction for the proposed method is roughly close to semi-active LQR. Clearly, the use of the proposed IBFC systems to control the behavior of the structure enable effective mitigation of peak response over other methods, while maintaining less inputs.

5.2 | Performance index

Reduction of the acceleration and the drift in a building during an excitation makes the residents feel comfortable and increases the safety of the structure. A scalar quantity, known as performance index (PI), was used to compare the performance of the different control systems. This approach and the method have also been used in previous studies.[45,56] To reflect the effects of either maximum drift or peak absolute acceleration response in the performance index, three indices, PI_t, PI_a, and PI_d, are defined by the form:

$$PI_t = w_a PI_a + w_d PI_d, \tag{25a}$$

$$PI_a = \frac{1}{n}\sum_{i=1}^{n}\left(\frac{a_{\max,i}}{a_{un,i}}\right), \tag{25b}$$

$$PI_d = \frac{1}{n}\sum_{i=1}^{n}\left(\frac{d_{\max,i}}{d_{\mathrm{un},i}}\right), \tag{25c}$$

where PI_a and PI_d represent the performance indices in terms of impacts of the maximum drift and peak absolute acceleration responses, respectively; PI_t is to account for the combined effects of both the maximum drift and peak absolute acceleration responses. For a specific system, a smaller value of these indices implies a better performance and more reduction in structural responses. n is the number of stories; $i$represents the degree of freedom; $d_{\max}$ and d_{un} are the maximum displacements corresponding to the ith degree of freedom for controlled and uncontrolled systems, respectively. Similarly, the parameters, $a_{\max}$ and a_{un}, are the peak absolute accelerations obtained from controlled and uncontrolled systems, respectively. The parameters, w_a and w_d, are weighting coefficients for acceleration and displacement, and they were selected equal to one in this study.

The PI_t for one-, five-, and ten-story buildings with IBFC system under the El Centro earthquake, illustrated in Figure 8, are reduced by 11, 12, and 9% as compared to the passive control with the optimum damping. With compared to the semi-active LQR system, the above reduction percentages are −5, +6, and −3%, respectively. Similar trend is observed for the case under the Northridge earthquake. Therefore, the maximum difference between the performance index for the semi-active LRQ control and the IBFC system is less than 6%, while the IBFC system is simpler in terms of less inputs.

To further investigate the performance of the proposed control method over other approaches under earthquakes with different magnitudes and peak ground acceleration, another

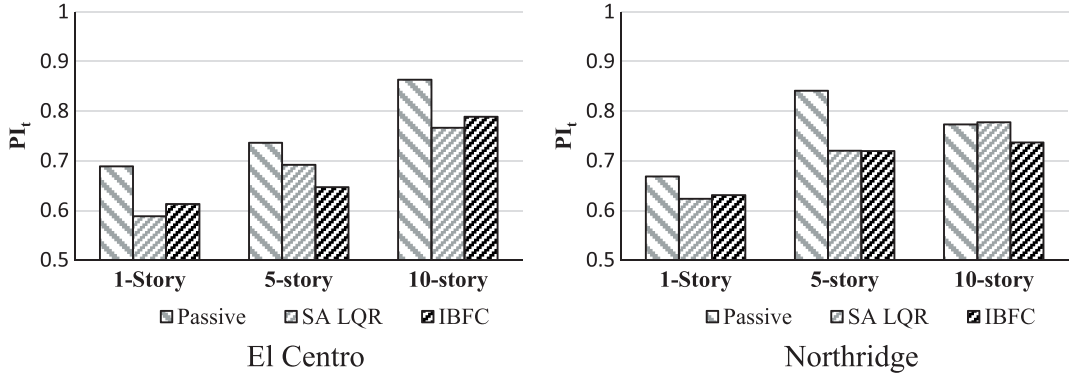

FIGURE 8 Performance index PIt of the buildings with passive, semi-active linear quadratic regulator (SA LQR), and integrated bracing flexibility compensator (IBFC) control

TABLE 3 Characteristics of the six earthquakes

Earthquake*	Station & Direction	Magnitude (M_w)	PGA (g)
1940 El Centro	El Centro Array no. 9 270°	7.2	0.21
1994 Northridge	Sylmar–Olive View Med FF 360°	6.7	0.84
1995 Kobe	H1170546.KOB 90°	7.2	0.63
1999 Chi-Chi	TCU068 N	7.6	0.36
1989 Loma Prieta	Hollister–South & Pine 0°	6.9	0.37
1971 San Fernando	Pacoima Dam 164°	6.6	1.22

*Reference: PEER Ground Motion Database (http://ngawest2.berkeley.edu/).

sets of analysis have been carried out on the five-story building under six historical earthquakes that are commonly used as external excitation,[19] as listed in Table 3. The control systems include (a) passive control with optimum damping (P_{opt}), (b) passive control with maximum damping (P_{Max}), (c) semi-active LQR (SA LQR), and (d) the proposed IBFC in this study.

Three performance indices in terms of the maximum drift, peak absolute acceleration, or overall are plotted over six earthquakes. As clearly shown in Figure 9a–c, the proposed IBFC has better performance in terms of reducing the peak absolute acceleration in the story level under the all six earthquakes as compared to the passive controls, while the overall performance is very similar when SA-LQR and IBFC controllers are used. Both of the passive systems have different performances under different excitations. Clearly, the passive control with maximum damping, due to less adapative capacity, cannot effectively reduce seismic response at most earthquake scenarios, particularly less effective to mitigation of peak absolute acceleration responses. Even though the optimally designed passive system considerably reduces the drift and acceleration under the El Centro, Northridge, and Kobe earthquakes, for the Chi-Chi, San Fernando, and Loma Prieta earthquakes, it is not as effective as SA-LQR and IBFC in reducing the drift response. The performance of the proposed controller is similar to the SA-LQR with +4.5, −4.0, +1.8, +11.6, 7.7, and 4.9% of difference in the overall performance index for the six earthquakes (shown in *x* axis from left to right). Further comparison of the proposed IBFC with the SA-LQR in terms of computation time, and energy consumed is addressed in Sections 5.3 and 5.4.

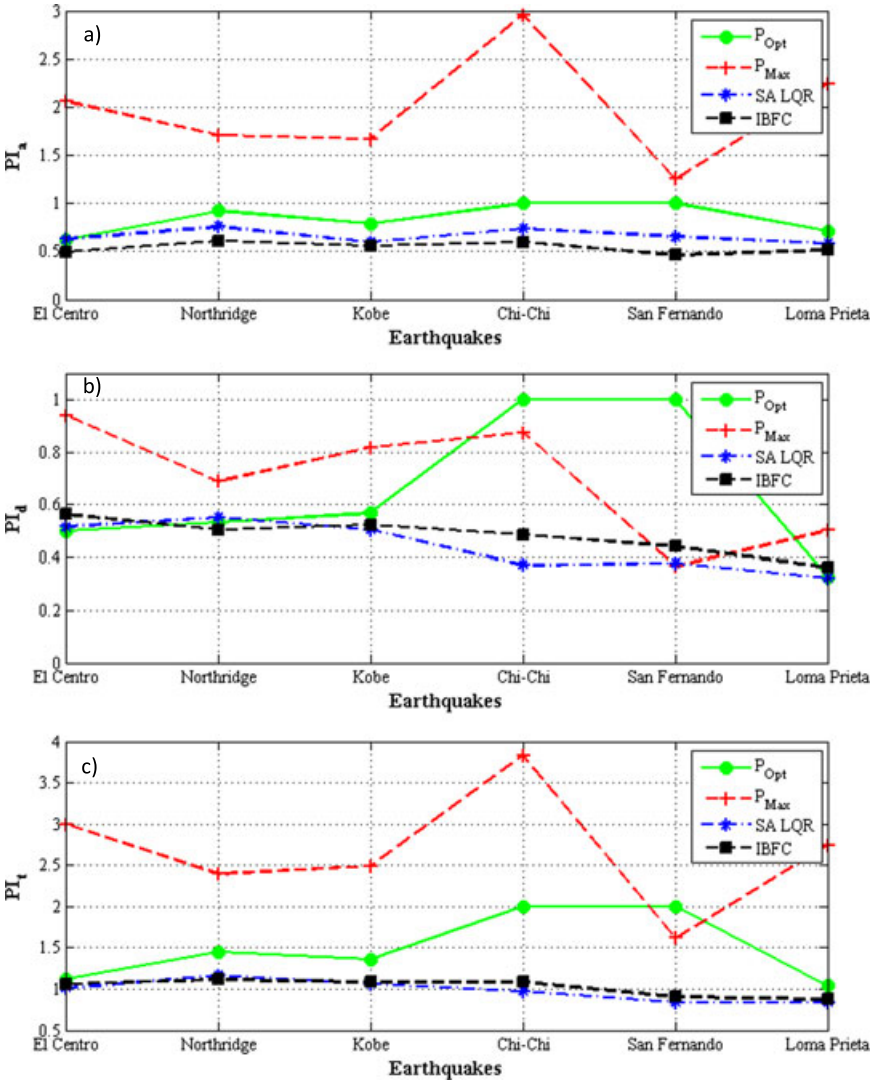

FIGURE 9 (a–c) Performance indices of the five-story building under six historical earthquakes. IBFC = integrated bracing flexibility compensator, SA LQR = semi-active linear quadratic regulator

5.3 | Time delay effects

Time delay directly affects the stability of structures.[57] By using the method,[58] the differential equations of the dynamic system are modified from Equation 13 by changing in variables that result in new equations, but without time delay, as follows:

$$[M]\{\ddot{x}(t)\} + [\boldsymbol{C}]\{\dot{x}(t)\} + [\boldsymbol{K}]\{x(t)\} = [\boldsymbol{D}]\{u(t-\lambda)\} - [\boldsymbol{M}]\{\boldsymbol{E}\}\ddot{x}_g(t), \quad (26)$$

where λ is the time delay; the actual controlling force for the new system is therefore computed with time delay effects. Figures 10–12 show the time delay effects for each building with the proposed control strategy under the El Centro earthquake.

These figures show the maximum drift and the peak absolute acceleration for different time delays within a range of 0.00 to 0.01 s. For each story level, the first two bars in the diagrams represent the uncontrolled system and the controlled system without delay, respectively. For the one-story building model, the extended range of time delay has been plotted for the responses to show the time delay influence on the performance of the system. As it is clear, for the drift response, a time delay less than approximately 0.02 s does not result in any differences in the response, and also for the other two buildings, for the time delays less than 0.005 s, there are no significant differences in the responses. By increasing the time delay, the differences become considerable; for example, the story drifts for a system with 0.01 s of time delay are less than the story drifts for the uncontrolled system; however, the peak absolute accelerations are greater compared to the uncontrolled system for the taller buildings.

As clearly illustrated in Figure 10a–b, a time delay longer than a specific value could lead to resonance and instability as compared to an uncontrolled system. Therefore, using controlling equations that decrease the computation tasks, with maintaining the overall performance, is an effective way to avoid undesired time delay effects and thus improve structural responses. The proposed controlling method does not need complicated computation operations, and it maintains the performance of the structure. This controller can be implemented into any microprocessors or an analog electrical circuit. The time delay in a logical circuit for the equation of the IBFC control is limited to few microseconds, but can reach to milliseconds by considering the time delays in other components of the system such as strain gauges and fluid flow control valves. According to the results, time delays within this range have no significant effects on inter-story drift and acceleration response.

In addition, to compare the response time of each algorithm, the total time consumed is determined as the mean value of computation time of 20 analyses with $dt = 0.001$s, as listed in Table 4. Clearly, the IBFC algorithm can significantly cut the computation time as compared to the LQR, by over 40% reduction for most multistory buildings. It can be envisioned that the proposed control algorithm could have a higher reduction in computation time for buildings with more complexities. Thus, as stated above, the less computation time could reduce time delay and thus reduce potential for resonance- or instability-induced issues.

5.4 | Energy of control force

In order to help understand the favorable features of the proposed method over the LQR method, energy of control is defined in accordance with the work of Amini et al[59] and used in this section, as well as the time-history of displacement and control force. Optimal control methods such as the LQR try to minimize the energy of the control through minimizing cost function in Equation 20. Energy of control is defined as

$$E_c(t) = \int_0^t F_d \dot{u} dt, \quad (27)$$

where $E_c(t)$ is the energy of control and F_d and $\dot{u}$ are the damper force and velocity, respectively.[59]

Figure 13a–c plot the time-history of displacement, control force, and energy of control at the top floor of the 10-story building under the El-Centro earthquake. The displacements predicted by the proposed method and the LQR control, illustrated Figure 13a, are almost identical to each other over the whole time history (i.e., maximum difference is about 0.5%), while the consumed energy (see Figure 13c) is significantly reduced using the proposed method. Despite the LQR control, the control force for the proposed method is smoother compared with the LQR method; thus, the proposed method is more reliable for short time delays as illustrated in the previous section. It is mainly because the damper force in the IBFC control algorithm is directly related to the inter-story velocity (see Equation 5).

6 | FURTHER DISCUSSIONS OF THE PROPOSED CONTROL METHOD AND ITS APPLICATIONS FOR PRACTICAL USE

As stated above, the proposed IBFC exhibits its favorable features over conventional control algorithms, particularly for input, time delay, computation time, and demanded energy. As parts of this study, further pilot laboratory tests will be conducted as the concept demonstration and will be documented in future publication. To address its practical use in design and implementation, we discuss the limitations and applicability of the proposed method below:

6.1.1 | Data collection

As critical input, sensor data will be crucial to provide information for controlling. Selection of proper sensors could be affected by their sensitivity, cost, and operating conditions. Although the conventional strain gauges are widely used to capture the strain, they are limited to their measuring range and are too fragile to survive under severe earthquake scenarios. The advanced sensors have recently become the

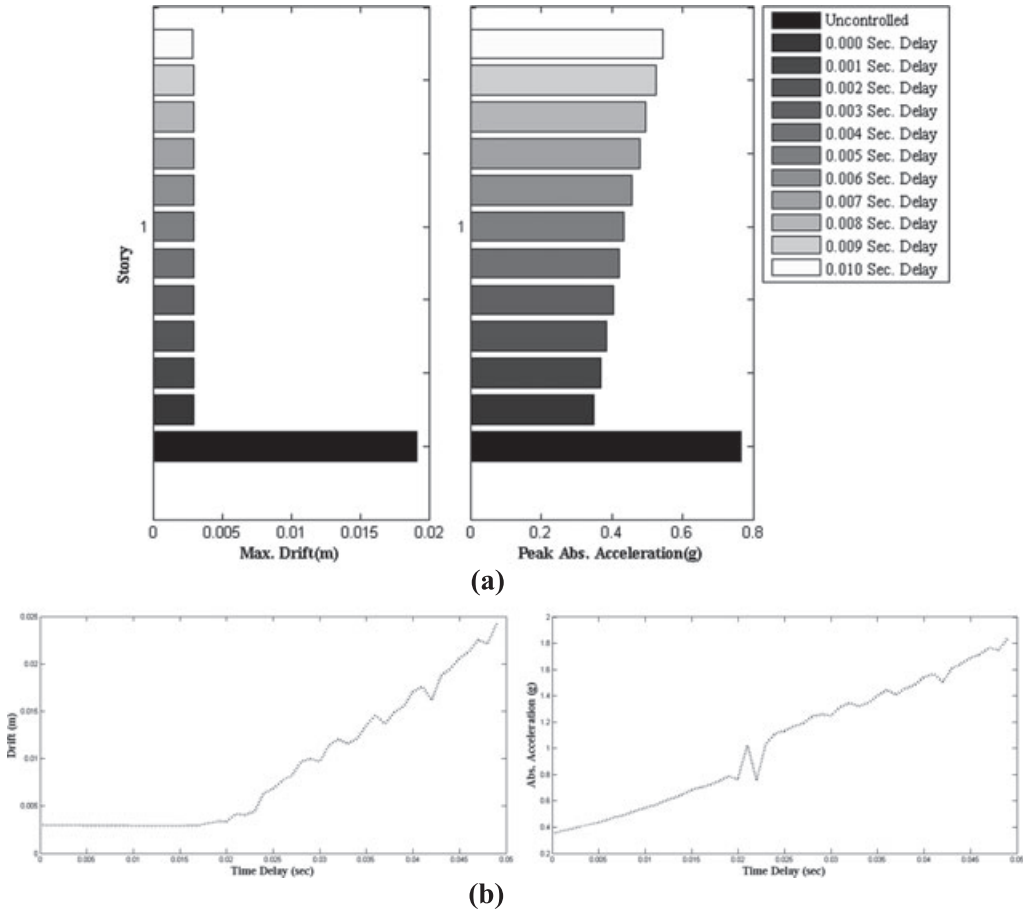

FIGURE 10 Maximum drift and peak absolute acceleration of the one-story building with time delay under the El Centro earthquake

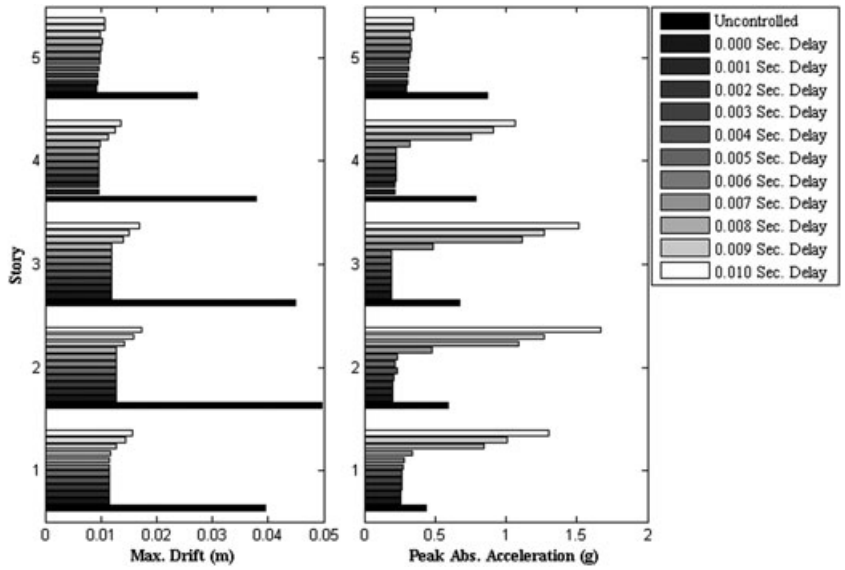

FIGURE 11 Maximum drift and peak absolute acceleration of the five-story building with time delay under the El Centro earthquake

emerging technologies in data collection, including surface mounted strain sensors, fiber optic sensors, and wireless strain sensors. These sensors could have much higher damage tolerance and particularly higher compatibility to long-term operating conditions or extreme events over conventional strain gauges.

6.1.2 | Effects of noise on collected data and data fusion for noise removal

Presence of noise in collected data is inevitable. Different methods have been proposed for offline and online noise filtering. Among them, the Kalman filter[60] has been used for studies on structural vibration control and damage

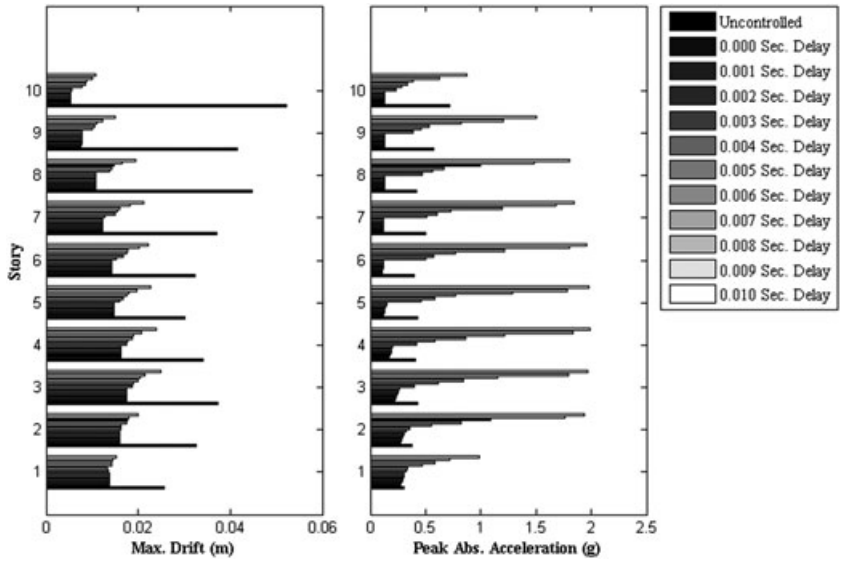

FIGURE 12 Maximum drift and peak absolute acceleration of the 10-story building with time delay under the El Centro earthquake

TABLE 4 Computation time for the controlled systems using LQR and IBFC (in seconds)

		LQR	IBFC	Reduction (%)
One-story	El Centro	1.285	0.843	−34
	Northridge	1.634	1.262	−23
Five-story	El Centro	3.844	2.090	−46
	Northridge	4.947	2.674	−46
Ten-story	El Centro	8.129	4.222	−48
	Northridge	10.489	5.350	−49

Note. IBFC = integrated bracing flexibility compensator, LQR = linear quadratic regulator.

identification.[61–64] The block diagram of typical application of Kalman filter is shown in Figure 14.

The Kalman filter tries to estimate the state vector z_i of the descerete control system for which the governing equation in state–space form is

$$z_i = \boldsymbol{A}z_{i-1} + \boldsymbol{B}u_{i-1} + w_{i-1}, \tag{28a}$$

$$y_i = \boldsymbol{C}z_i + v_{i,} \tag{28b}$$

where y_i is the measurement vector; $\boldsymbol{C}$ is output matrix; and w_i and v_i represent the process and measurement noise, respectively, which are assumed to be independent white Gaussian noises.

$$p(w) \sim N(0, \boldsymbol{Q}), \tag{29a}$$

$$p(v) \sim N(0, \boldsymbol{R}). \tag{29b}$$

where $\boldsymbol{Q}$ and $\boldsymbol{R}$ are the process and measurement noise covariance. The recursive discrete Kalman filter cycle includes a set of mathematical equations for time update and measurement update, which is given in Figure 15 in summary.

Two cases are considered to demonstrate the effectiveness in reducing the noise in real-time using the Kalman filter. For both cases, $Q = 10^{-9} \times \boldsymbol{I}_{n \times n}$, $R_{\text{Case-I}} = 10^{-5} \times \boldsymbol{I}_{n \times n}$, and $R_{\text{Case-II}} = 10^{-6} \times \boldsymbol{I}_{n \times n}$. Figure 16 shows the measured and filtered displacement responses at the first story of the five-story building under El Centro earthquake. Figure 16b shows the zoomed plot for the selected time window, and it is clearly

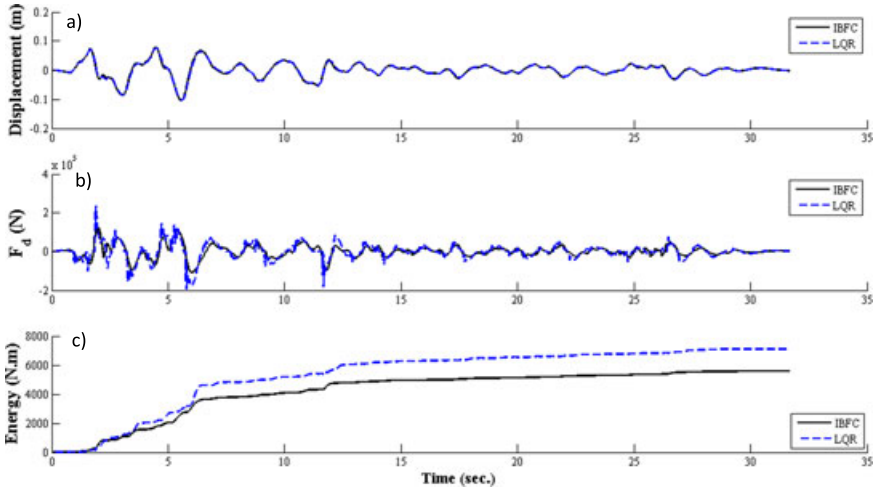

FIGURE 13 (a–c) Controlled displacement, control force, and energy of control at the top floor of the 10-story building under the El Centro earthquake. IBFC = integrated bracing flexibility compensator, LQR = linear quadratic regulator

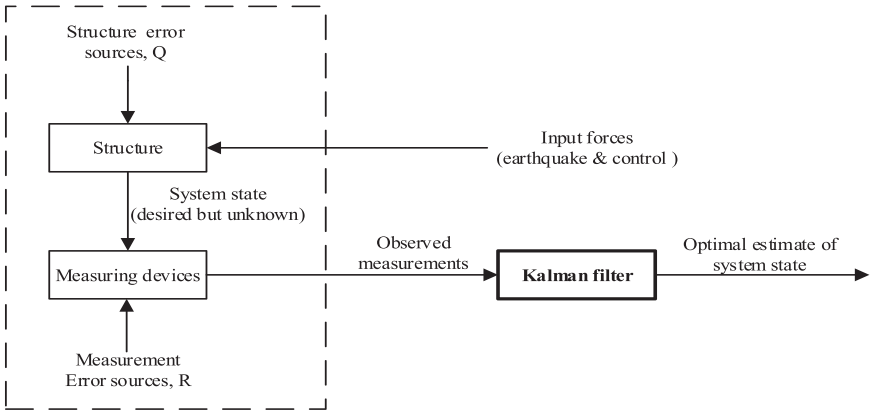

FIGURE 14 Typical application of the Kalman filter

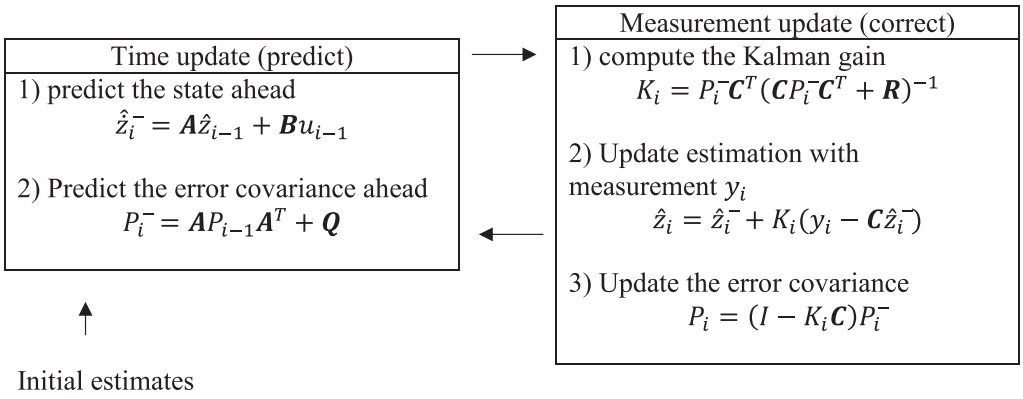

FIGURE 15 Flowchart of the Kalman filter algorithm

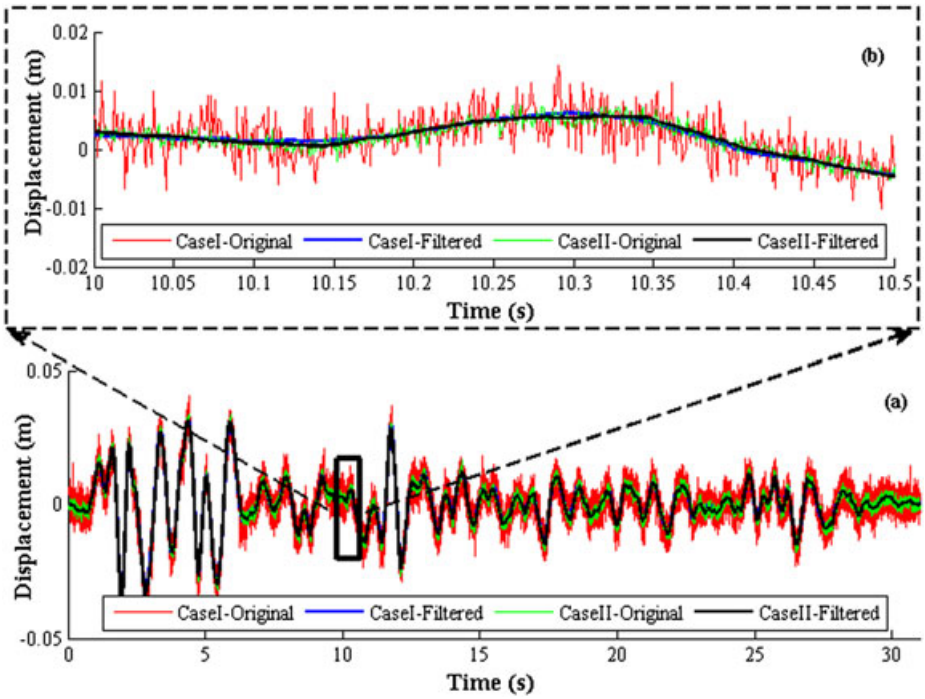

FIGURE 16 Displacement response of first story of five-story building before and after Kalman filter under El Centro earthquake loading: (a) the time history and (b) zoomed time window

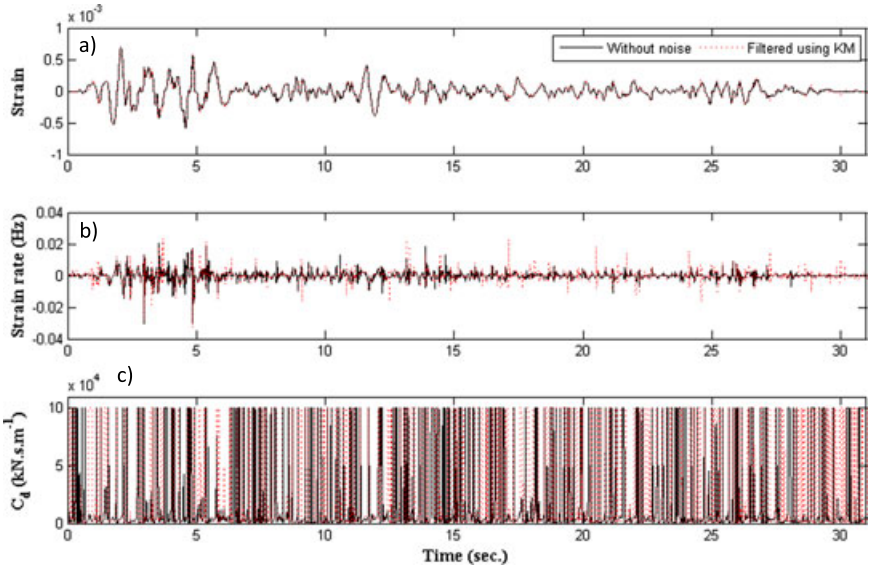

FIGURE 17 (a–c) Strain and strain rate at the fourth floor of the five-story building under El Centro earthquake

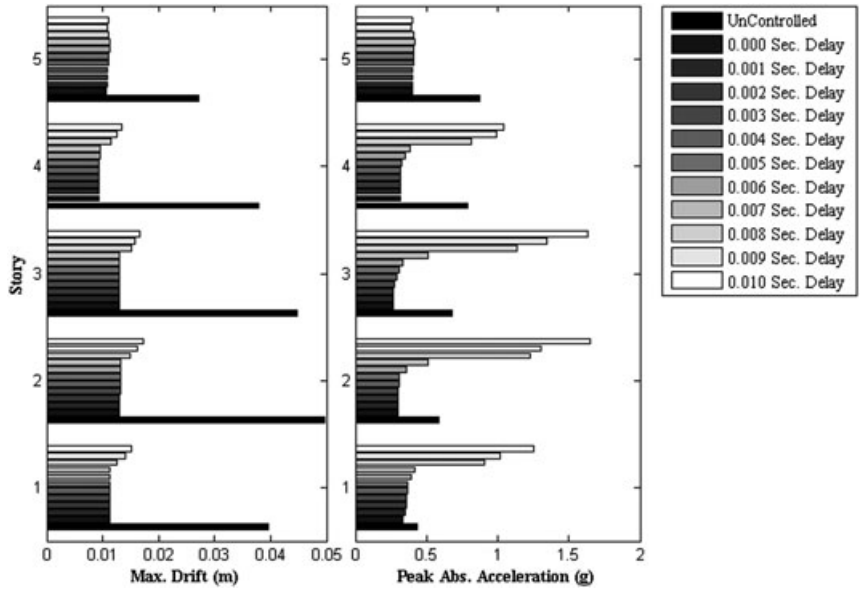

FIGURE 18 Maximum drift and peak absolute acceleration of the five-story building with time delay under the El Centro earthquake (using Kalman filter for noise reduction)

that the Kalman filter significantly reduces the noise effects in the measured displacement, and for both cases, the filtered data match well with each other.

In addition, in order to provide a better understanding about the proposed method, the strain and strain rate of brace members at the top floor of the 10-story building is shown in Figure 17. Clearly, the filtered strain is in good agreement with the data without noise interference, as shown in Figure 17a. Also, Figure 17b shows the filtered strain rate and initial data without noise still match well, although there are some variation points with peak shifts. The corresponding damping coefficient of the control device is also illustrated in Figure 17c.

Furthermore, the effect of time delay on the system with noise was also considered in this study. Figure 18 shows the time delay effect on the response of the five-story building for which the Kalman filter has been used for noise reduction (Case 1). By comparing to the system without noise shown in Figure 11, there is minimal change in time delay effects when using the data treated by Kalman filter, as shown in Figure 18.

7 | CONCLUSIONS

In this study, a new developed simple semi-active damper was investigated to enhance seismic performance for the V-braced multistory buildings. In addition to its simplicity, the proposed controlling strategy demands fewer input to gain the damping coefficient and, accordingly, the controlling force. To evaluate the performance of the proposed method,

we create and analyze three analytical models different earthquake scenarios. The results demonstrate that without an active control algorithm and with less input data, the proposed damper can significantly mitigate the seismic response of structures. In addition to the general advantages of the semi-active systems, the proposed semi-active damper provides favorable features as follows:

1. **More high performance through less input parameters and less computation time:** The input data for the proposed control system are the strain of the bracing members, which could be captured by mounted sensors. Also, results reveal that the proposed control algorithm has higher performance with over 40% reduction in overall computation time as compared to the semi-active LQR control.
2. **Non-centralized system:** This system can be considered as a non-centralized system. By installing separate controllers for each damper, the system sustains its functionality, even when a certain controller may not work properly. Moreover, active control systems are mainly dependent on feedback data from dynamic properties of structure. Therefore, any possible subjective error in estimating those parameters or nonlinear response of the structures may cause adverse impact on their reliability. Differently, the proposed system that includes the algorithm with adaptive automation can minimize such errors through automated parameter generation and thus provide more robust strategies in structural control.
3. **Time delay effects:** Time delay can result in instability of structure, if exceeds critical limits. Because the proposed control system is simple, even with the analog electrical circuits, the time delay in applying the control force is not long enough to cause major differences in the responses.
4. **Energy of control:** As a measure of potential applications of the proposed method, the energy of control is calculated and compared with the semi-active LQR control results. The IBFC system provides almost same behavior as the system with LQR control, but with less energy of control.
5. **Data fusion and noise reduction:** The data fusion for raw sensor data is crucial to implement the control systems, because the collected data could be contaminated by various operating conditions. Clearly, the Kalman filter can effectively reduce the noise effects and avoid potential error in estimating controlling parameters.

ACKNOWLEDGMENTS

The authors gratefully acknowledge the financial support provided by Ozbun Economic Development Award, ND DOC Venture I Grant and US DOT (FAR0025913). The results, discussion, and opinions reflected in this paper are those of the authors only and do not necessarily represent those of the sponsor.

REFERENCES

[1] A. Kaveh, T. Bakhshpoori, M. Azimi, *Struct. Des Tall Special Buildings* **2015**, *24*, 210.

[2] O. Lavan, *Struct. Control Health Monit.* **2015**, *22*, 484.

[3] G. Ghodrati Amiri, M. Azimi, E. Darvishan, *Scientia Iranica, Trans. Civil Eng. 20*, 1695. Number 2013

[4] A. Mosleh, M. S. Razzaghi, J. Jara, H. Varum, *Int. J. Adv. Struct. Eng.* **2016**, *8*, 1.

[5] A. Mosleh, J. Jara, H. Varum, *J. Struct. Eng. Geo-Tech.* **2015**, *5*, 1.

[6] A. Mosleh, H. Rodrigues, H. Varum, A. Costa, A. Arêde, *Structure 7*, 1 .8// 2016

[7] A. Nicknam, A. Mosleh, H. Hamidi Jamnani, in *The Proceedings of the Twelfth East Asia-Pacific Conference on Structural Engineering and Construction – EASEC12*, **2011**

[8] A. V. Srinivasan, D. M. McFarland, *Smart Structures: Analysis and Design*, Cambridge University Press, Cambridge, United Kingdom **2000**.

[9] F. Y. Cheng, H. Jiang, K. Lou, *Smart Structures: Innovative Systems for Seismic Response Control*, CRC Press **2008**.

[10] C. S. Teodorescu, S. Diop, I. Politopoulos, M. Benidir, in *Control & Automation (MED), 2013 21st Mediterranean Conference on*, **2013**, pp. 545–550.

[11] F. Oliveira, P. G. d. Morais, A. Suleman, *Procedia Eng.* **2015**, *114*, 401.

[12] D. A. Shook, P. N. Roschke, O. E. Ozbulut, *Struct. Control Health Monit.* **2008**, *15*, 746.

[13] O. Ozbulut, S. Daghash, M. Sherif, *J. Mater. Civ. Eng.* **2016**, *28*(4).

[14] C. Xu, K. Huo, Z. Ren, R. Xiong, T. Yang, *Adv. Mater. Res.* **2013**, *706–708*, 530.

[15] N. Krishnamra, E. Limsuwan, J. Dawe, *ACI Struct. J.* **2010**, *107*, 563.

[16] Y.-S. C. J. P. Eunsoo Choi, C. Baik-Soon, *Struct. J.* **2010**, *107*.

[17] L. F. K. Murat Engindeniz, Z. Abdul-Hamid, *Struct. J.* **2005**, *102*.

[18] S. C. Goel, W.-C. Liao, M. R. Bayat, S.-H. Chao, *Struct. Design Tall Special Buildings* **2010**, *19*, 115.

[19] O. E. Ozbulut, M. Bitaraf, S. Hurlebaus, *Eng. Struct.* **2011**, *33*, 3143.

[20] M. Bitaraf, S. Hurlebaus, *Eng. Struct.* **2013**, *56*, 2107.

[21] N. R. Fisco, H. Adeli, *Scientia Iranica, Trans. Civil Eng.* **2011**, *18*, 275.

[22] N. R. Fisco, H. Adeli, *Scientia Iranica, Trans. Civil Eng.* **2011**, *18*, 285.

[23] E. Nazarimofrad, S. M. Zahrai, *Soil Dyn. Earthq. Eng.* **2016**, *89*, 100.

[24] G. W. Housner, L. A. Bergman, T. K. Caughey, A. G. Chassiakos, R. O. Claus, S. F. Masri, R. E. Skelton, T. T. Soong, B. F. Spencer, J. T. P. Yao, *J. Eng. Mech.* **1997**, *123*, 897.

[25] M. Abdeddaim, A. Ounis, N. Djedoui, M. K. Shrimali, *Asian J. Civil Eng.* **2016**, *7*, 985.

[26] M. Abdeddaim, A. Ounis, N. Djedoui, M. K. Shrimali, *J. Civ. Struct. Health Monit.* **2016**, *6*, 603.

[27] M. K. Bhardwaj, T. K. Datta, *J. Struct. Eng.* **2006**, *132*, 791.

[28] F. Amini, S. A. Mohajeri, M. Javanbakht, *Smart Mater. Struct.* **2015**, *24*. p. 105002

[29] A. Y. Fallah, T. Taghikhany, *Smart Mater. Struct.* **2015**, *24*, 125030.

[30] S. Mohammadi, S. Hatam, *JVC/J. Vib. Control* **2015**, *21*, 21.

[31] B. F. Spencer, T. T. Soong, in *Proceedings of International Post SMIRT Conference on Seismic Isolation, Passive*, **1999**.

[32] N. Kurata, T. Kobori, M. Takahashi, N. Niwa, H. Midorikawa, *Earthq. Eng. Struct. Dyn.* **1999**, *28*, 1427.

[33] A. Nishitani, Y. Nitta, Y. Ikeda, *J. Struct. Eng.* **2003**, *129*, 933.

[34] T. T. Soong, B. F. Spencer Jr., *Eng. Struct.* **2002**, *24*, 243.

[35] H. Kurino, J. Tagami, K. Shimizu, T. Kobori, *J. Struct. Eng.* **2003**, *129*, 895.

[36] Y. Ikeda, *Struct. Control Health Monit.* **2009**, *16*, 703.

[37] O. Cundumi, L. E. Suárez, *J. Mech. Mater. Struct.* **2007**, *2*, 1639.

[38] K. Kazemi Bidokhti, H. Moharrami, A. Fayezi, *Struct. Control Health Monit.* **2012**, *19*, 417.

[39] M.-H. Shih, W.-P. Sung, *Sadhana* **2014**, *39*, 123.

[40] N. Kurata, T. Kobori, M. Takahashi, T. Ishibashi, N. Niwa, J. Tagami, H. Midorikawa, *Earthq. Eng. Struct. Dyn.* **2000**, *29*, 629.

[41] C. G. Go, C. H. Sui, M. H. Shih, W. P. Sung, *J. Vib. Control* **2010**, *16*, 2195.

[42] H. Kurino, S. Orui, K. Shimizu, *J. Disaster Res.* **2009**, *4*, 253.

[43] F. Oliveira, P. Gil de Morais, A. Suleman, presented at the ICSI 2015 The 1st International Conference on Structural Integrity Funchal, Madeira, Portugal, **2015**.

[44] B. F. Spencer Jr., S. Nagarajaiah, *J. Struct. Eng.* **2003**, *129*, 845.

[45] M. Ahmadizadeh, *Struct. Control Health Monit.* **2007**, *14*, 858.

[46] T. T. Soong, *Active structural control: theory and practice*, Longman Scientific & Technical **1990**.

[47] A. K. Chopra, *Dynamics of Structures: Theory and Applications to Earthquake Engineering*, Prentice Hall, Englewood Cliffs, New Jersey **2012**.

[48] B. Basu, S. Nagarajaiah, *Eng. Struct.* **2008**, *30*, 2470.

[49] S. F. Ali, A. Ramaswamy, *Struct. Control Health Monit.* **2009**, *16*, 564.

[50] A. M. Aly, A. Zasso, F. Resta, *Smart Materials Res.* **2011**, *2011*.

[51] N. Mohajer Rahbari, B. Farahmand Azar, S. Talatahari, H. Safari, *Struct. Control Health Monit.* **2013**, *20*, 1021.

[52] A. M. Aly, *Struct. Des. Tall Special Build.* **2014**, *23*, 664.

[53] F. Amini, M. Z. Samani, *Comput. Aided Civ. Inf. Eng.* **2014**, *29*, 464.

[54] S. N. Deshmukh, N. K. Chandiramani, *Shock. Vib.* **2014**, *2014*, 12.

[55] Y. Shi, T. C. Becker, S. Furukawa, E. Sato, M. Nakashima, *Earthq. Eng. Struct. Dyn.* **2014**, *43*, 1265.

[56] M. Bitaraf, S. Hurlebaus, L. R. Barroso, *Comput. Aided Civ. Inf. Eng.* **2012**, *27*, 48.

[57] H. Temimi, M. Ben-Romdhane, S. El-Borgi, Y.-J. Cha, *Int. J. Struct. Stab. Dyn.* **2016**, *16*(7), 1550031.

[58] G. P. Cai, J. Z. Huang, S. X. Yang, *Comput. Struct.* **2003**, *81*, 1539.

[59] F. Amini, N. K. Hazaveh, A. A. Rad, *Comput. Aided Civ. Inf. Eng.* **2013**, *28*, 542.

[60] R. E. Kalman, *J. Basic Eng.* **1960**, *82*, 35.

[61] S. Gerist, M. R. Maheri, *J. Sound Vib.* **2016**, *384*, 210.

[62] S. Gerist, S. S. Naseralavib, E. Salajegheh, *Int. J. Optimization Civil Eng.* **2012**, *2*, 301.

[63] S. S. Naseralavi, S. Gerist, E. Salajeghegh, J. Salajeghegh, *Int. J. Struct. Stab. Dyn.* **2013**, *13*. p. 1350024

[64] A. R. Vosoughi, S. Gerist, *Compos. Struct.* **2014**, *118*, 68.

How to cite this article: Azimi M, Rasoulnia A, Lin Z, Pan H. Improved semi-active control algorithm for hydraulic damper-based braced buildings. *Struct Control Health Monit*. 2017;24:e1991. https://doi.org/10.1002/stc.1991